Measurements of fuel distribution and flame structure in kerosene-fuelled combustors using planar laser-induced fluorescence and OH* emissions

M. Orain[†*], F. Grisch[†], H. Verdier[††]
[*] Physics, Instrumentation and Sensing Department
ONERA
Palaiseau, France
[††] Combustion Chambers Department
Turbomeca
Bordes, France

Abstract

Kerosene-PLIF was successfully applied to a LPP injector for various operating conditions (air temperature up to 730 K, pressure between 1 and 5 bars, equivalence ratio between 0.44 and 0.74) at firing conditions. 2D-maps of instantaneous kerosene vapour spatial distribution in the combustor were measured. Chemiluminescence emissions from OH* radical were also recorded to determine the global flame shape and to correlate it with fuel distribution. At atmospheric pressure, the flame is lifted from the injector outlet at low and medium temperatures; however, the flame is stable. At high temperatures, the flame is located immediately at the exit of the LPP premixing duct. At 5 bars, kerosene fuel disappears at medium axial distance downstream from the LPP injector, and this indicates that combustion starts close to the outlet of the injection system. OH* chemiluminescence shows that the flame is present at the outlet of the injector. Kerosene spatial distribution exhibits numerous wrinkled structures, and this indicates that the flame is highly turbulent. As a result, the position of the flame front exhibits large spatial and temporal fluctuations, and so does the location of kerosene removal. Consequently, kerosene and OH* mean spatial distributions are located at similar positions. Nonetheless, no instabilities or flame flapping is noted.

Introduction

Increasingly stringent regulations on pollutant emissions, such as NO_x, CO_x and soot, require to improve combustion efficiency and overall operability of kerosene-fuelled aeronautical gas turbines. Among key parameters likely to fulfil these goals, the injection system is one of them where substantial improvements can still be achieved. It is well known that atomisation of liquid jets (shear-coaxial injectors) occurs via different physical processes compared to break-up of liquid sheets (film injectors), which often results in different droplet size, velocity and density [1,2]. Therefore, optimising the atomisation of liquid fuel into fine droplets and their subsequent evaporation is of great importance for fuel spatial distribution within the combustor [3,4]. Efficient mixing between preheated combustion air and fuel vapour generated by droplet evaporation is also crucial to combustion efficiency. First, in terms of pollutant emissions which can be greatly reduced if the spatial distribution of air/fuel mixture in the combustor is homogeneous with lean equivalence ratio. This yields lower flame temperature (1500-1800 K), hence lower NO_x emissions, and the absence of fuel-rich pockets leads to reduced soot formation. Second, in terms of combustion instabilities which are known to partly depend on temporal and spatial inhomogeneities of the air/fuel mixture in the combustor. Such instabilities are naturally not compatible with standards of reliability, durability and drivability required for aircrafts engines, and, therefore, must be avoided.

Over the last two decades, intensive research has been dedicated to improve existing injection systems and to imagine innovative designs. This has led to new concepts like multipoint, LP (Lean Premixed) and LPP (Lean Premixed Prevaporised) injectors which contribute to match the targeted goals of future regulations on pollutants emissions [5]. The principle of these injectors is to atomise the liquid fuel into small droplets which evaporate to a large extent, and mix the subsequent fuel vapour with air in a prevaporising/premixing duct, in order to obtain a fairly homogeneous air/fuel mixture before combustion occurs. Many experiments have used laser-based techniques to determine the influence of parameters like droplet size and velocity, air temperature, fuel and air flowrates on the performances of such injectors [6,7]. However, these studies were mainly focused on the spatial distribution of liquid phase in the combustor, and the evolution of droplet size at different locations from the injector exit was used to estimate fuel evaporation [8,9]. Indeed, only few experiments were performed to characterise fuel vapour phase [10-12]. In addition, results were typically obtained with surrogate fuels or added tracers which were not necessarily representative of typical fuels used in aircraft engines (i.e. kerosene). There-

* Corresponding author: mikael.orain@onera.fr

fore, it may be that the conclusions drawn from these experiments were biased by the type of fuel they used, because of the different evaporation behaviour and combustion processes of surrogates or tracers compared to that of real fuels. Only very few examples of studies performed with laser-based diagnostics directly applied to kerosene vapour are available in the literature [13,14]. Unfortunately, these results were only qualitative, because kerosene spectroscopy was not properly established despite the pioneering work of Löfström et al. [15]. Arnold et al. [16] also applied planar laser-induced fluorescence (PLIF) to fuel-oil detection in gas turbines for temperature between 360 and 486 °C at atmospheric pressure. The authors have indicated that PLIF could enable equivalence ratio measurements within a 25 % error. Recently, Baranger et al. [17] have thoroughly investigated photophysics of kerosene for various conditions of temperature, pressure and oxygen molar fraction, with a 266 nm excitation wavelength. Dependence of kerosene fluorescence on the above parameters was measured and the molecular species responsible for this fluorescence were identified. Using the spectroscopic results of Baranger et al. [17], Orain et al. [18] have derived a quantitative strategy for measuring local equivalence ratio in kerosene-fuelled gas turbines using PLIF-kerosene. The technique was applied to a LPP injector operating with jet A1 fuel at atmospheric pressure for non-reactive conditions, at temperature between 500 and 730 K and overall equivalence ratio in the range 0.12–0.44. Influence of these parameters on the spatial distribution of local equivalence ratio in the combustor was investigated. However, these experiments were performed without combustion, at low pressure and, therefore, there was a need to assess the capability of the technique to measure fuel vapour concentration at high pressure firing conditions. Characterising the performances of aircraft injectors also requires the determination of the flame structure and flame reaction rate, which gives information about combustion efficiency depending on operating conditions. This can be classically performed using chemiluminescence from OH* radical and the technique has already been applied to large pressures [19-21].

The goal of the present experiments was to measure fuel spatial distribution using PLIF-kerosene and flame structure using chemiluminescence from OH* radical in a fired combustor operating with jet A1 fuel. The techniques were successfully applied at temperature between 580 and 730 K and pressure up to 5 bars. The paper comprises five sections. The next section briefly recalls the photophysics of aromatics fluorescence for application to kerosene-fuelled combustors. The third section presents the combustor facility and describes the optical set-up. In the fourth section, the optical techniques are subsequently applied to a kerosene-fuelled injector. Finally, the paper ends with a summary of the main findings.

Planar Laser-Induced Fluorescence for kerosene vapour measurements

In a typical PLIF experiment, the flow is illuminated by a laser sheet which wavelength is tuned to excite a particular transition of a molecular tracer, which can be a species naturally-produced in the flow (CH, OH, C_2, CO, …) or seeded into the flow (I_2, O_2, NO, aldehydes, ketones, aromatics …). A fraction of the molecules in the lower energy level absorbs the incident light and is promoted to a higher energy level. Some of the excited molecules photodissociate or return to equilibrium, either by emitting photons or by transferring the excess of energy through non-radiative decay processes (collisional quenching, intersystem crossing, internal conversion or vibrational relaxation). For a weak laser excitation, the fluorescence signal intensity can be expressed as [22]:

$$I = \eta_{opt} \frac{E}{hc/\lambda} V_c N_{abs} \sigma(\lambda, T) \frac{k_f}{k_f + k_{nr} + \sum_q k_q X_q} \quad (1)$$

where η_{opt} is the overall efficiency of the collection optics, E is the laser fluence (J/cm^2), hc/λ is the energy (J) of a photon at the excitation wavelength λ and V_c is the collection volume (cm^3). Quantities that may vary with gas dynamic parameters (temperature T, total pressure P, and species composition) are N_{abs}, the number density of absorbing molecules (cm^{-3}); σ, the molecular absorption cross section of the molecule (cm^2); k_f, the spontaneous emission rate; k_{nr}, the upper-level decay rate owing to collisionless processes (such as intersystem crossing, photodissociation or vibrational relaxation) and k_q, the collisional-quenching rate. X_q is defined as the molar fraction of the quenching species. In the case of kerosene, which is mainly composed of aliphatic and aromatic molecules, fluorescence typically arises from the excitation of aromatics [17]. It is well known from the literature that oxygen is the main quencher for aromatics fluorescence [23,24] and that other species like H_2O, CO or CO_2 have little influence. Therefore X_q will be denoted as X_{O2} in the following.

The expression of Eq. 1 can be used to derive strategies for imaging quantities such as equivalence ratio and temperature, which completely characterise spray evaporation, only in the mixing regions of non-burning and burning sprays, upstream from the flame front. In these specific regions, oxygen can be considered as the main quencher of kerosene fluorescence and, therefore, Eq. 1 can be applied. Visualisation of mixing process requires simultaneous 2D-imaging of fuel and oxygen concentrations in the flow with a temporal resolution faster than the timescales of mixing and chemical reaction. Most simply, the fluorescence signal is a specific function of T, X_{O2} and X_{fuel} for a particular excitation wavelength. Detection of fluorescence from aromatics with one excitation wavelength over two specific spectral ranges can provide dual-parameter imaging, yielding for example

equivalence ratio in addition to temperature. Detection of kerosene and di-aromatics fluorescence signals on two separate ICCD cameras with appropriate optical filters a possible measurement strategy because of their different temperature and oxygen dependencies. Using experimentally-determined behaviour of kerosene fluorescence [17], along with a calibration point in a reference flow where thermodynamic parameters are well known, an iterative processing routine of both instantaneous fluorescence signals, combined with the closure relation for species composition (i.e., $X_{fuel}+X_{O2}+X_{N2}=1$) is then used to determine the desired quantities. Note that this data reduction implies that the ratio between mono-aromatics and di-aromatics remains constant in the experiments. This assumption remains valid for temperatures up to 1100-1300 K, where kerosene pyrolysis is observed.

Additional spectroscopic measurements to those of Baranger et al. [17] have been performed in a test cell at high temperature and pressure. For instance, Fig. 1 represents the evolution of integrated fluorescence from di-aromatics with temperature and pressure under N_2 atmosphere. As can be seen, fluorescence intensity decreases by about 55 % as temperature increases from 450 to 700 K, which corresponds to the range of interest for PLIF measurements in gas turbines. This indicates that temperature has some influence on di-aromatics fluorescence, although the signal reduction with temperature remains somehow limited. Figure 1b shows that fluorescence from di-aromatics increases with pressure for different temperatures, and the gradient is stronger below 0.5 MPa. Together with results from Fig. 1a, this allows to estimate the evolution of fluorescence signal with temperature *and* pressure for a given concentration of kerosene vapour. For example, fluorescence intensity per molecule is reduced by a factor of 2 as temperature and pressure change from (450 K, 0.5 MPa) to (700 K, 2.0 MPa). This indicates that fluorescence signals remain easily detectable at high temperature and pressure, and gives us confidence about the applicability of kerosene-PLIF to operating conditions representative of aircraft engines.

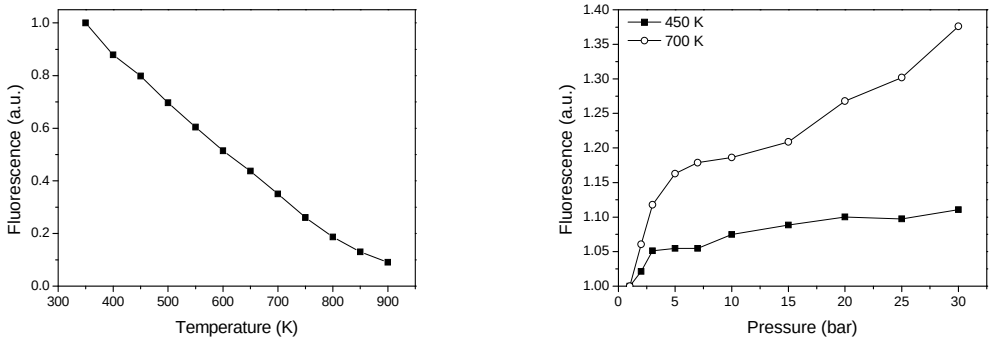

(a) (b)

Figure 1. Evolution of di-aromatics integrated fluorescence in N_2 with temperature at atmospheric pressure (a) and with pressure for two temperatures (b).

Experimental set-up

Combustor facility

Figure 2 represents a picture of the test rig which allows to perform measurements with optical diagnostics at pressure up to 10 bars. This bench consists of a heat exchanger which can preheat air up to 1000 K for air flowrates up to 100 g/s. The heater was connected to the combustor which comprised three parts made of stainless steel. The first part was a cylinder which contains glass beads in order to homogenise the airflow. The fuel supply line was located on the cylinder centreline and it was encapsulated in a water-cooled jacket to ensure that the temperature of liquid kerosene remained constant during experiments. The water jacket itself was also covered with ceramics to minimise heat losses. The LPP system was fixed at the top of the fuel supply line and connected to a metallic anti-recirculation plate placed across the section of the combustor, in order to have a flat wall at the inlet of the optical sector. The second part of the combustor corresponded to the water-cooled visualisation sector. It was equipped with three optical access made of UV-silica windows, one of which was used for laser access and the two others for detecting kerosene fluorescence and OH* chemiluminescence with ICCD cameras. Optical access was specifically designed so that fluorescence and chemiluminescence could be collected directly at the outlet of the prevaporising duct. The exit of the combustor is equipped with a sonic throttle which can be partly obstructed by a needle in order to control the pressure inside the combustor. Finally, exhaust gases are collected by a fan. Air was supplied by the laboratory compressor and its flowrate was controlled by a mass flowmeter in the range 0-100 g/s with 0.2 % uncertainty. Liquid kerosene was stored in a pressurised tank and its flowrate was controlled by a mass flowmeter in the range 0-13 kg/h with 0.2 % uncertainty. For a given pressure condition, air flowrate was kept constant and overall equivalence ratio (Φ_0) was varied between 0.44 and 0.74. Air inlet temperature ranged from 580 to 730 K and pressure was between 1 and 5 bars.

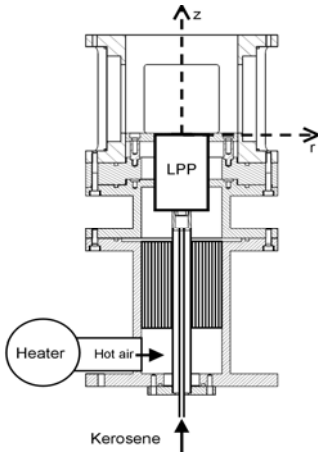

Figure 2. Schematic of the combustor facility.

Optical set-up

Kerosene-PLIF experiments used a single-excitation scheme which comprises a frequency-quadrupled Nd:YAG laser generating 8 ns, 50 mJ pulses at 266 nm. The laser beam was transformed into a collimated sheet using a combination of cylindrical and spherical lenses. Two cylindrical lenses formed a cylindrical telescope which spread the beam into a collimated, 50 mm high, sheet and the spherical lens focused the sheet to a 130 μm waist. The laser sheet impacted the kerosene/air spray, and kerosene fluorescence was recorded with a 16-bit ICCD camera (IMAX-512, Roper). The camera has a 512×512 pixel CCD array, a temporal gate of 40 ns and a framing rate of 4 Hz. It is equipped with a *f*/4.1, *f*=94 mm, achromatic UV lens and a high-pass filter (WG 280, Schott) to collect kerosene fluorescence. The camera was interfaced to a personal computer used to control the camera and record the images. A 50×50 mm^2 area of the flow was imaged by the ICCD camera, so that the spatial resolution was about 100 μm per pixel along the dimensions of the image and 130 μm in the third dimension (i.e. perpendicular to the laser sheet). The spatial resolution was measured on a target of known size where lines with known thickness were drawn. Raw fluorescence images were corrected for background luminosity, non-uniformities in the collection optics and inhomogeneity in the laser sheet profile. An average background image was acquired with the laser on in hot air. Subtraction of this image from the fluorescence image accounted for laser scattering and other background luminosity. An average background image was also acquired with the laser off and the flame on, in order to remove flame chemiluminescence emissions from the raw fluorescence images.

For OH* chemiluminescence measurements, the same camera as for kerosene-PLIF was used. The camera had a temporal gate of 10 μs and it was equipped with a band-pass filter centred at 310 nm (FWHM=30 nm, transmission=20 %) to record the chemiluminescence from OH* radicals only. As opposed to kerosene-PLIF measurements which are temporally and spatially resolved, OH* emission measurements have lower temporal resolution and are spatially averaged over the line-of-sight. An average background image was acquired with the flame off in hot air. Subtraction of this image from the raw chemiluminescence images accounted for the noise of the ICCD camera.

Figure 3a presents a typical instantaneous raw image of kerosene fluorescence after illumination of the flow in the combustor by the laser sheet from top to bottom. The bright dots, representing large intensities, correspond to droplets, while fuel vapour is displayed with a false colorscale. The gain of the camera was adjusted to keep the energy recorded by the array detector proportional to the fluorescence signal issued from the liquid and gas phases, which prevented the ICCD camera from local saturation and blooming induced by the liquid kerosene fluorescence. For each flow condition, 200 single-shot images were acquired with the ICCD camera and the maps of mean kerosene fluorescence and mean chemiluminescence from OH* radical presented in this article result from the average over these 200 single-shots. Raw images were corrected as indicated previously. Finally, with the present experiments, it was necessary to add an extra routine which takes account of the presence of kerosene droplets in the flow. Due to the difference of density between the liquid and vapour phases of kerosene, fluorescence signals were significantly larger for the liquid phase. As a result, there was a strong intensity gradient between a droplet and its surrounding vapour. We took advantage of this feature to identify the location of droplets and to eliminate the fluorescence signal from the liquid phase which was initially set to zero. The fluorescence signal at the droplet location was then interpolated over the droplet area using the value of fluorescence intensity from kerosene vapour at the first pixel around the droplet both in the radial and axial directions. Example of this processing is shown in Fig. 3b along one direction only.

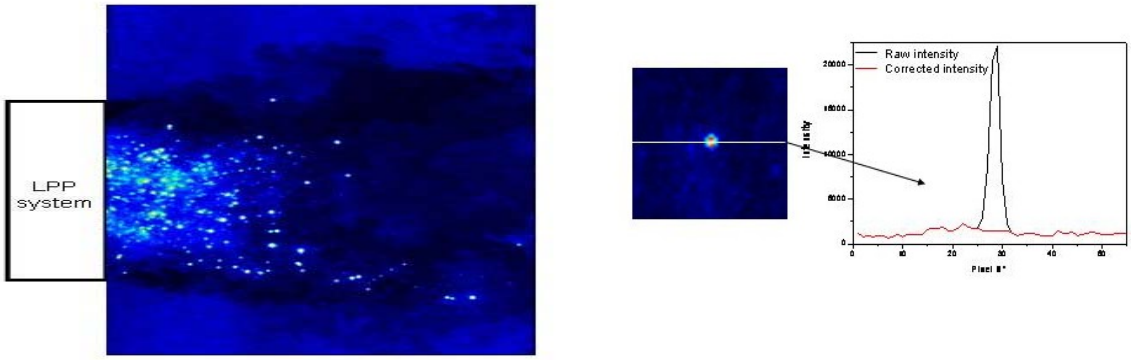

(a) (b)

Figure 3. Fluorescence intensity emitted by kerosene vapour and droplets in the combustor (a), procedure used to interpolate fluorescence intensity over a droplet area (b).

Results

This section presents kerosene-PLIF and OH* chemiluminescence measurements at the outlet of the LPP injector for different operating conditions. In the following figures, the kerosene/air flow propagates from left to right and the injector is schematised by the green rectangle on the left of each image. In the kerosene-PLIF experiments, the laser sheet propagates from the top to the bottom of the images and it is located on the vertical axis of the combustor. Both kerosene-PLIF and OH* images are represented with a black-to-red colorscale, where red colour represents the maximum intensity of either kerosene fluorescence or OH* chemiluminescence.

Influence of air inlet temperature

Figures 4 and 5 represent kerosene-PLIF and OH* emission images for air inlet temperature of 580 K and Φ_0=0.60. As can be seen, kerosene fuel is fairly homogeneously distributed all over the LPP injector section, suggesting fairly good mixing between kerosene and air in the injection system. Little radial expansion of the kerosene/air jet is noted at the outlet of the injection system. The rms of kerosene spatial distribution exhibits higher values at the edges of the injector, possibly due to swirl effects close to the injector walls. There is an area with low values of rms close to the centreline over about 15 mm downstream from the injector, indicating that kerosene fuel is present all the time with similar concentrations at that position. Almost no droplets are visible, suggesting good atomisation and vaporisation processes. Moreover, kerosene fuel is observed at large axial distance downstream from the injector on both instantaneous and mean fluorescence images, which indicates that kerosene does not burn right at the outlet of the LPP injector. This is confirmed by OH* images where almost no chemiluminescence signal is observed over about 40-50 mm downstream from the injector (figures 5a and 5b). This indicates that the flame is largely lifted from the injection system with this condition (average lift-off distance ~ 40 mm). The flame is blue and seems to be distributed in volume all over the combustor section. Flame length is estimated to be in excess of 15 cm. However, the flame is stable and no flapping is observed. This suggests that with this condition, the injector operates without flame instabilities, despite the flame is lifted.

Figures 6 and 7 represent kerosene-PLIF and OH* emission images for air inlet temperature of 730 K and Φ_0=0.44. By contrast with lower inlet temperature, kerosene fuel is mainly located at the edges of the kerosene/air jet. Little radial expansion of the kerosene/air jet is noted. A sharp disappearance of kerosene vapour corresponding to the instantaneous position of the flame front is clearly visible in figures 6a and 6b. OH* chemiluminescence shows that the flame is attached at the outlet of the LPP injection system. Nonetheless, visual observation shows that the flame is already developing inside the premixing duct of the LPP injector. It is stable and no flame flapping is observed. The flame is located on the inner side of the cone delimitating kerosene fuel. This result indicates that kerosene burns close to the centreline and, therefore, it cannot be observed at that position. In addition, it is interesting to remark that the mean images of kerosene fluorescence and OH* chemiluminescence are perfectly complementary. Indeed, some angle dissymmetry is observed between the upper and the lower part of both figures 6d and 7a. Moreover, superimposition of these figures shows that kerosene spatial extent can perfectly stick into the regions at the periphery of the flame mean position. The flame has a bright colour with a jet shape of limited radial expansion, its length is strongly reduced compared to conditions with lower air temperature and it is approximately about 6–7 cm. It is noted that with this air inlet temperature, the injector can operate at low overall equivalence ratio, which suggests that large air preheating increases the flammability range of the injector.

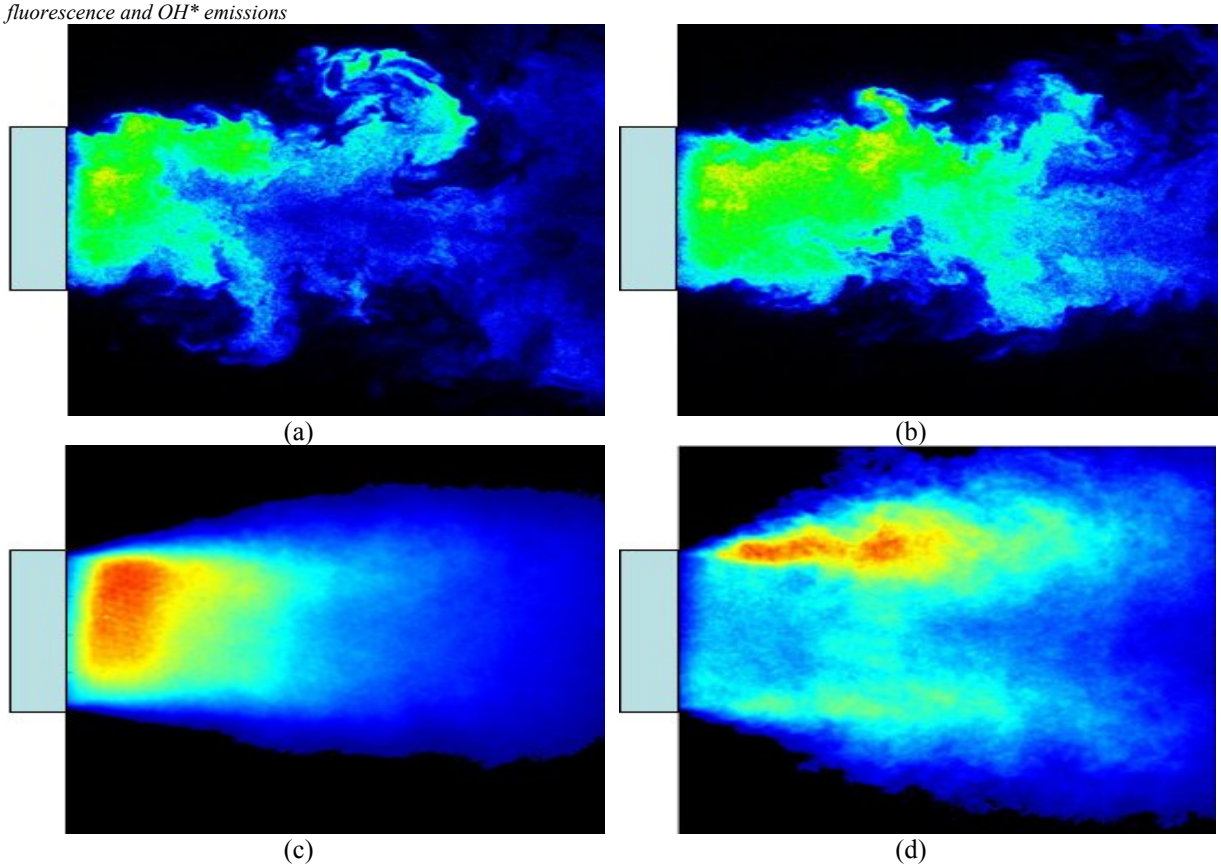

Figure 4. Instantaneous images of kerosene fluorescence (a) and (b), mean and rms images of kerosene spatial distribution (c) and (d), at the outlet of the LPP injector, for 580 K, 1 bar, Φ_0=0.60.

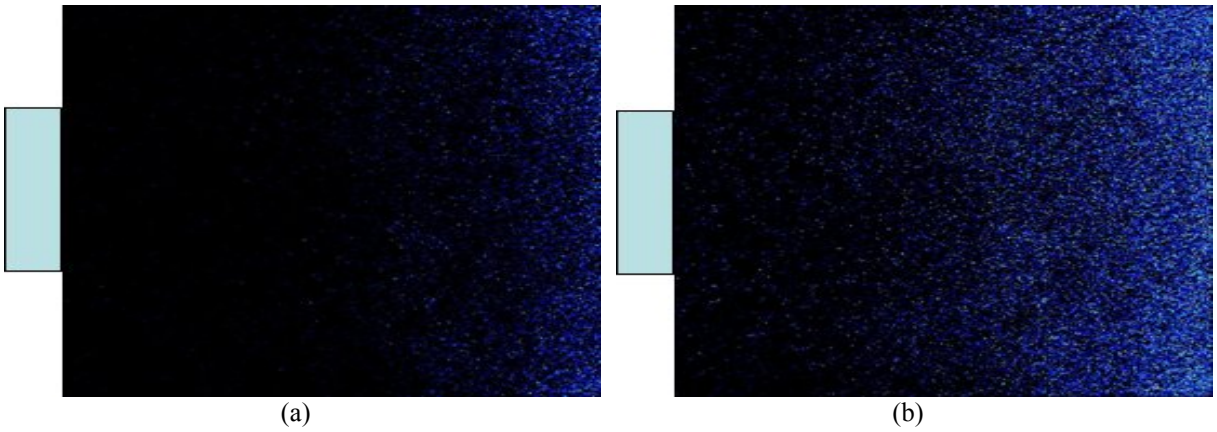

Figure 5. Mean and rms images of OH* chemiluminescence spatial distribution (a) and (b), at the outlet of the LPP injector, for 580 K, 1 bar, Φ_0=0.60.

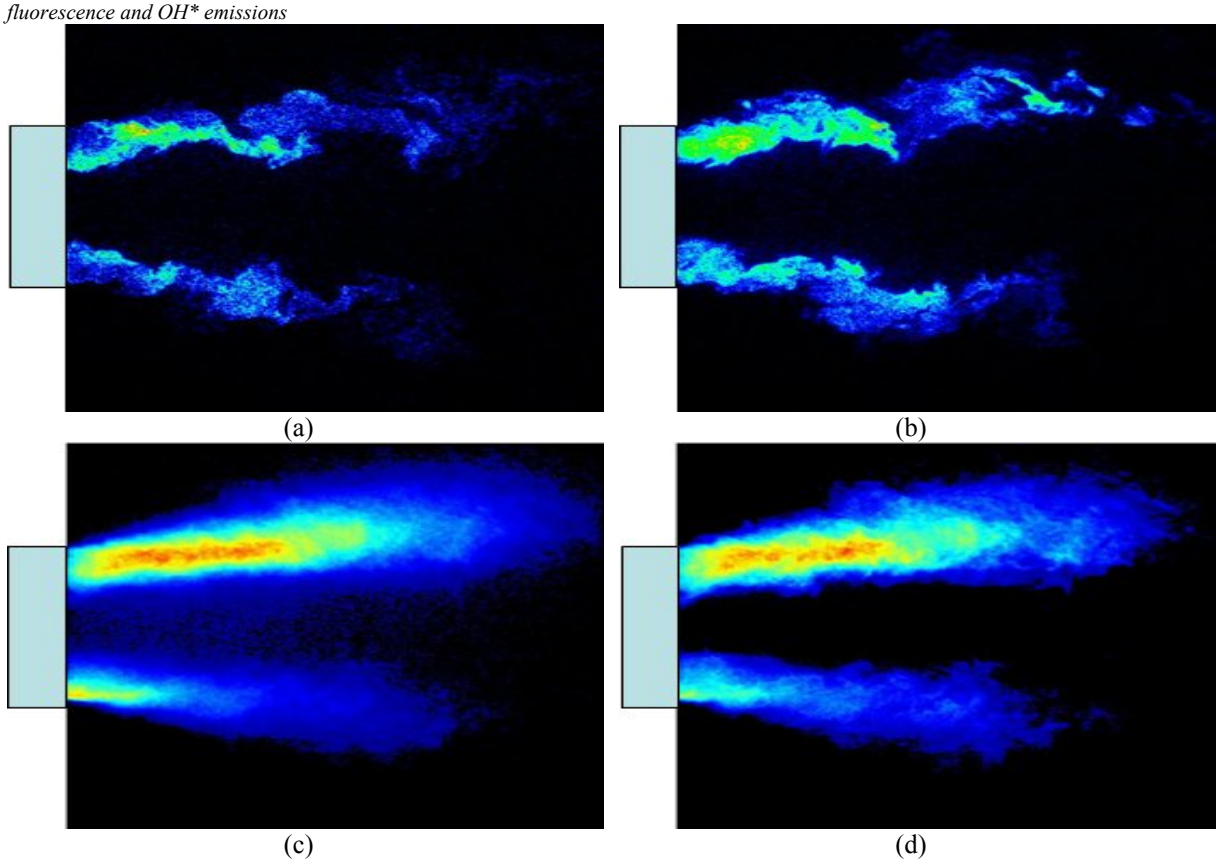

Figure 6. Instantaneous images of kerosene fluorescence (a) and (b), mean and rms images of kerosene spatial distribution (c) and (d), at the outlet of the LPP injector, for 730 K, 1 bar, Φ_0=0.44.

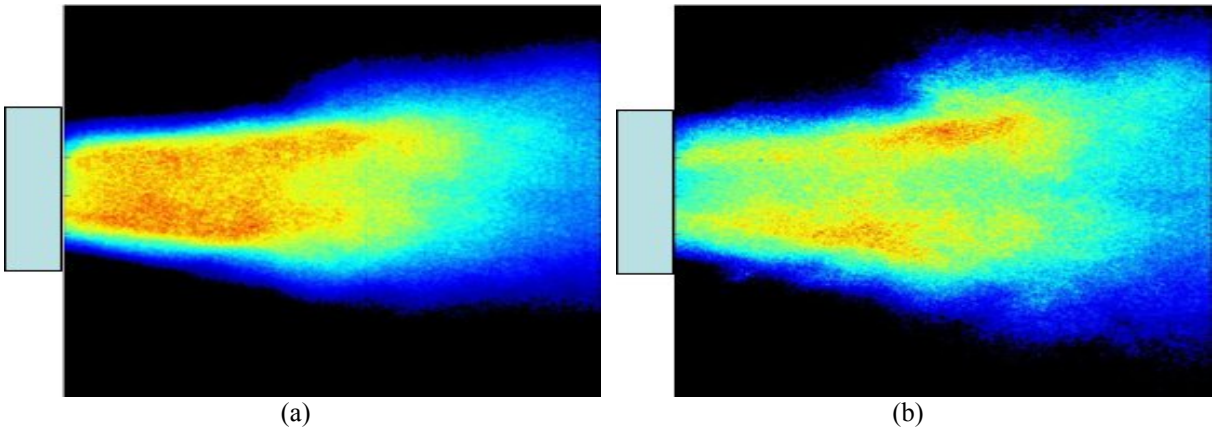

Figure 7. Mean and rms images of OH* chemiluminescence spatial distribution (a) and (b), at the outlet of the LPP injector, for 730 K, 1 bar, Φ_0=0.44.

Influence of pressure

Kerosene-PLIF and OH* emission images are displayed in figures 8 to 11 for air inlet temperature of 650 K, Φ_0=0.44 and pressure of 1 and 5 bars. At 1 bar, results are similar to observations for 580 K. Kerosene fuel is fairly homogeneously distributed all over the LPP injector section and shows little radial expansion. The rms of kerosene spatial distribution exhibits higher values at the edges of the injector. The flame is lifted by about 40 mm, but stable; it is blue and distributed in volume all over the combustor section. Flame length is approximately about 10-15 cm. By contrast, at 5 bars, OH* chemiluminescence shows that the flame is located immediately at the outlet of the injector. However, it is likely that the flame is already developing inside the premixing duct of the LPP injector. No instabilities or flame flapping is noted. The flame exhibits a bright colour and its length is less than 8–9 cm. This result suggests that, with this injector, pressure has a positive influence on flame stabilisation and leads to reduced flame length. Kerosene fuel is fairly homogeneously distributed all over the

LPP injector section and the kerosene/air jet exhibits little radial expansion. Increasing pressure from 1 to 5 bars led the extent of the kerosene spatial distribution to be significantly reduced. The liquid fuel disappears at medium axial distance downstream from the LPP injector, and this indicates that combustion starts close to the outlet of the injection system. It is noted that kerosene and OH* mean spatial distributions are located at similar positions in the flow. At a first sight, it may be intriguing that kerosene and flame are both present all over the section for about 20 mm downstream from the injector. However, there is no contradiction between these results. Indeed, as can be seen for example in figure 10a, kerosene spatial distribution exhibits many wrinkled structures, indicating that the flame is highly turbulent. Therefore, the position of the flame front constantly changes both spatially and temporally, so does the location of kerosene removal. As a result, kerosene and OH* mean spatial distribution are located at similar positions. In addition, it should be noted that OH* emission measurements are spatially averaged over the line-of-sight, as opposed to planar measurements (over 130 µm thickness) with kerosene-PLIF, and this introduces additional uncertainty on the interpretation of OH* chemiluminescence images.

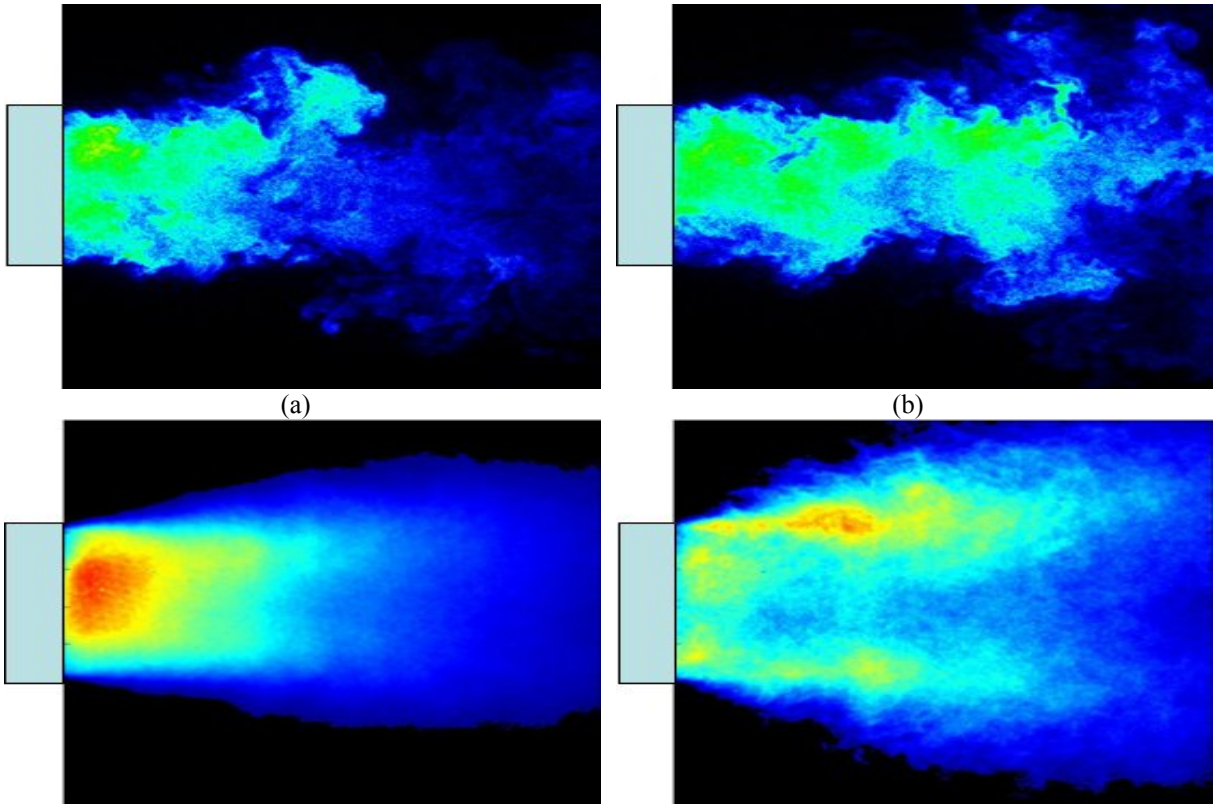

Figure 8. Instantaneous images of kerosene fluorescence (a) and (b), mean and rms images of kerosene spatial distribution (c) and (d), at the outlet of the LPP injector, for 650 K, 1 bar, Φ_0=0.44.

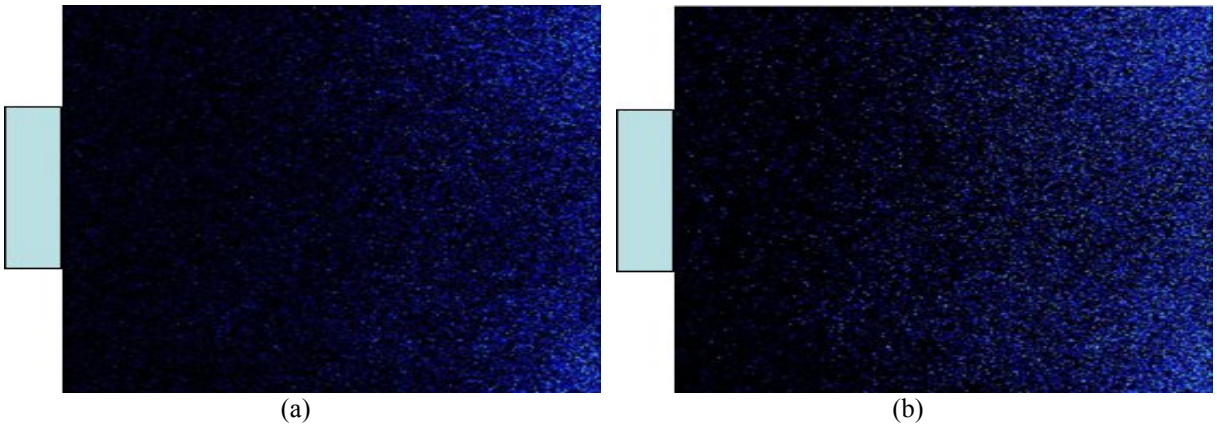

Figure 9. Mean and rms images of OH* chemiluminescence spatial distribution (a) and (b), at the outlet of the LPP injector, for 650 K, 1 bar, Φ_0=0.44.

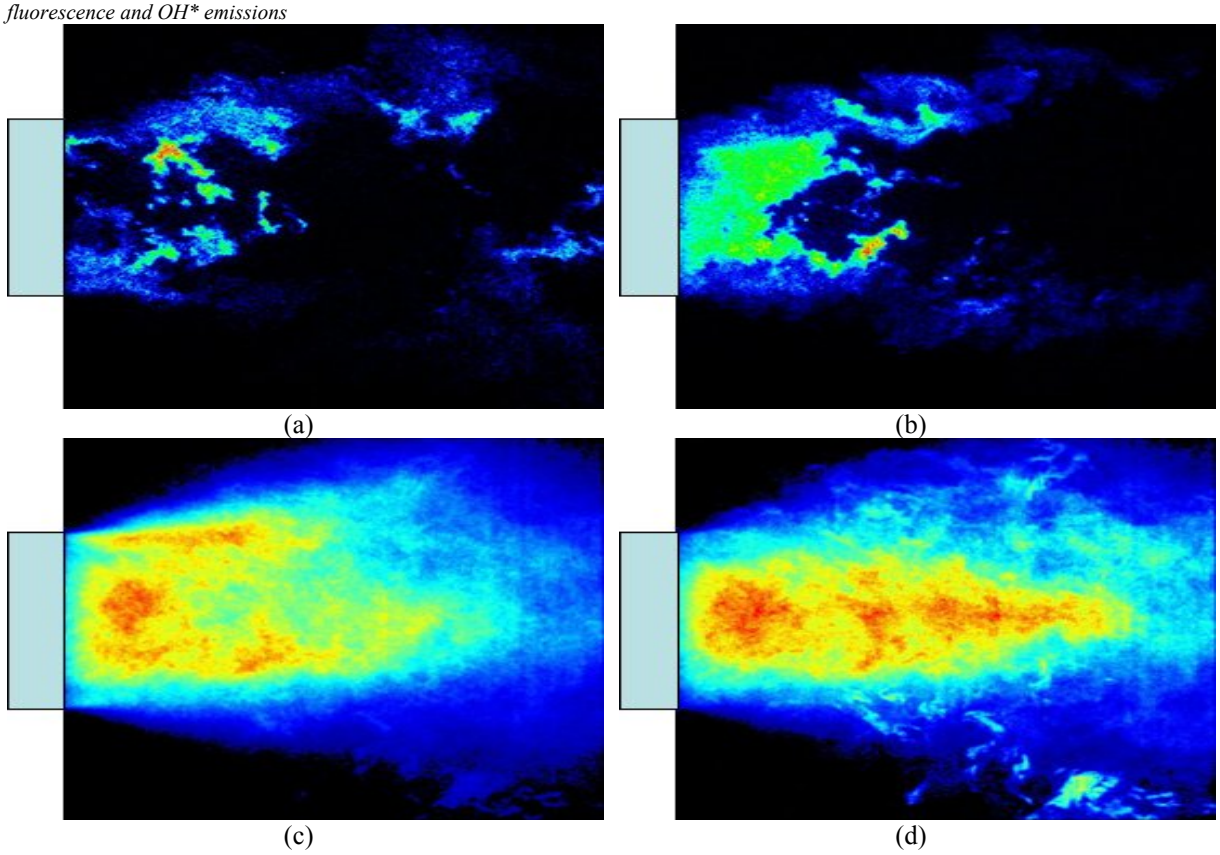

Figure 10. Instantaneous images of kerosene fluorescence (a) and (b), mean and rms images of kerosene spatial distribution (c) and (d), at the outlet of the LPP injector, for 650 K, 5 bars, $\Phi_0=0.44$.

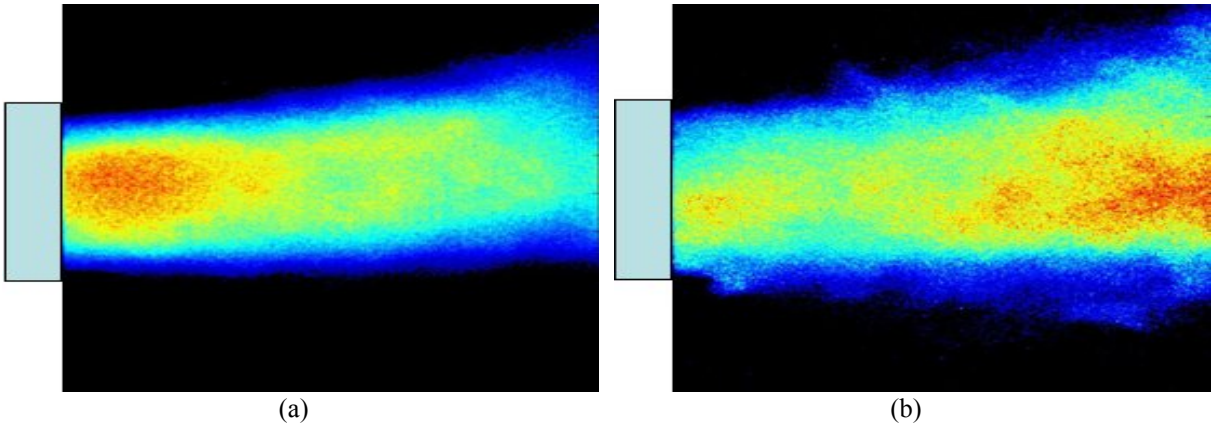

Figure 11. Mean and rms images of OH* chemiluminescence spatial distribution (a) and (b), at the outlet of the LPP injector, for 650 K, 5 bars, Φ_0=0.44.

Conclusions

Measurements of fuel spatial distribution using kerosene-PLIF and flame structure using OH* chemiluminescence were performed at the outlet of a Lean Premixed Prevaporised (LPP) injection system from Turbomeca. Experiments were carried out at firing conditions, for air inlet temperature between 580 K and 730 K, with combustor pressure in the range 1 to 5 bars, for different equivalence ratios. Results are as follows.

- At atmospheric pressure, flames are lifted by ~ 40 mm from the injector for 580 and 650 K, whereas the flames are already developing inside the premixing duct of the LPP injector for 730 K. By contrast, at 5 bars, for all temperatures, flames are likely to already develop inside the premixing duct of the LPP injector. Flames are highly turbulent and the flame front is wrinkled.

- Both at 1 and 5 bars, kerosene fuel is homogeneously distributed at the injector outlet over its section for 580 and 650 K, whereas it is located at the edges of the injector for 730 K (due to fuel consumption close to the centreline).
- Little radial expansion of kerosene/air jet is noted.
- Combustion is stable and no instabilities or flame flapping are observed.

As already mentioned, OH* emission measurements are spatially averaged over the line-of-sight, as opposed to planar measurements with kerosene-PLIF, and this introduces additional uncertainty on the interpretation of OH* chemiluminescence images. A possibility to improve the characterisation of the injector operation is to combine simultaneously kerosene-PLIF and OH-PLIF techniques to measure instantaneous maps of kerosene and OH radical at the same time. Such measurements would help to correlate the fuel spatial distribution and the position of the flame front. In addition, it is also necessary to measure simultaneously maps of kerosene and pollutants such as NO and CO produced in the flame to correlate the formation regions of pollutants with the local concentration of fuel. Such experimental data are useful for the validation of numerical simulations and to improve their predicting capabilities.

Acknowledgments
This work was performed within the "NEW Aero engine Core concepts" program sponsored by the European Union under grant N° FP6-2005-Aero-1 with D. Chiron as program monitor and MTU Aero Engines as coordinator.

References
[1] M. Pilch, C.A. Erdman, *Int. J. Multiphase Flow* 13: 741-757 (1987).
[2] A.H. Lefebvre, *Atomization and sprays*, 1st Edition, Hemisphere Publishing, 1989.
[3] A.H. Lefebvre, *J. Eng. Gas Turb. Power* 117: 617-654 (1995).
[4] A.H. Lefebvre, *Gas turbines combustion*, 2nd Edition, Taylor & Francis, 1999.
[5] S.M. Correa, *Combust. Sci. and Tech.* 87: 329-362 (1992).
[6] C. Löfström, J. Engström, M. Richter, C.F. Kaminski, P. Johansson, K. Nyholm, J. Hult, J. Nygren, M. Aldén, ASME paper N° 2000-GT-0124 (2000).
[7] D.A. Greenhalgh, *Proceeding of the Institution of Mechanical Engineers, Part A: Journal of Power and Energy* 214: 367-376 (2000).
[8] Y. Michou, I.S. Carvahlo, C. Chauveau, I. Gökalp, AIAA paper N° 1999-332 (1999).
[9] J. Becker, C. Hassa, *J. Eng. Gas Turb. Power* 125: 901-908 (2003).
[10] J.H. Stufflebeam, D.W. Kendrick, W.A. Sowa, T.S. Snyder, *J. Eng. Gas Turb. Power* 124: 39-45 (2002).
[11] D. Galley, A. Pubill Melsio, S. Ducruix, F. Lacas, D. Veynante, AIAA paper N° 2004-4032 (2004).
[12] H. Krämer, F. Dinkelacker, A. Leipertz, ASME paper N° 99-GT-135 (1999).
[13] Y.R. Hicks, R.J. Locke, R.C. Anderson, M. Zaller, H.J. Schock, AIAA Paper N° 97-2837 (1997).
[14] Y.R. Hicks, R.J. Locke, R.C. Anderson, NASA report No. TM-2000-210377.
[15] C. Löfström, H. Kaaling, M. Aldén, *26th Int. Symp. on Comb.*, Naples, Italy, August 1996, pp. 2787-2793.
[16] A. Arnold, R. Bombach, W. Hubschmid, A. Inauen, B. Käppeli, *Exp. in Fluids* 29: 468-477 (2000).
[17] P. Baranger, M. Orain, F. Grisch, AIAA paper N° 2005-828 (2005).
[18] M. Orain, H. Verdier, F. Grisch, *13th International Symposium on Application of Laser Techniques to Fluid Mechanics*, Lisbon, Portugal, June 2006, pp. 1220.
[19] B. Higgins, M.Q. McQuay, F. Lacas, J.C. Rolon, N. Darabiha, S. Candel, *Fuel* 80: 67-74 (2001).
[20] Y. Ikeda, J. Kojima, H. Hashimoto, *29th Int. Symp. on Comb.*, Sapporo, Japan, August 2002, pp. 1495-1501.
[21] T.M. Muruganandam, B.H. Kim, M.R. Morrell, V. Nori, M. Patel, B.W. Romig, J.M. Seitzman, *30th Int. Symp. on Comb.*, Chicago, USA, August 2004, pp. 1601-1609.
[22] R.K. Hanson, *21st Int. Symp. on Comb.*, Munich, Germany, August 1986, pp. 1677-1691.
[23] J.B. Birks, *Photophysics of aromatic molecules*, Wiley-Interscience, London, 1970.
[24] W. Koban, J.D. Koch, R.K. Hanson, C. Schulz, *Appl. Phys. B* 80: 777-784 (2005).